JOURNAL OF SOLID STATE CHEMISTRY 96, 97–107 (1992)

Lanthanum Magnesium Aluminate (LMA) and Its Derivatives: An Example of Laser Materials Engineering

R. COLLONGUES[1] AND D. VIVIEN

Laboratoire de Chimie Appliquée de l'Etat Solide, URA 1466 du CNRS, E.N.S.C.P., 11 rue Pierre et Marie Curie, 75231 Paris cedex 05, France

Received July 12, 1991

A new family of lanthanide-activated laser materials based on magnetoplumbite structural type is studied. By some convenient chemical modifications it is possible to improve the laser characteristics of the starting material such as laser efficiency, thermal behavior, tunability range, and wavelengths of emission. A new way of activating solids using ionic exchange is also described and applied to a set of compounds close to the magnetoplumbite family.

Introduction

From the discovery, in 1960, of the laser effect in ruby, a number of other laser materials have been identified. From A. A. Kaminskii (*1*) 320 crystalline lasers are known; 290 use a lanthanide as active ion and among them 143 are activated with neodymium ion Nd^{3+}. Some neodymium doped aluminates such as yttrium aluminium garnet (YAG : Nd), yttrium aluminium perovskite (YAP : Nd), and yttrium lithium fluoride (YLF : Nd) are of considerable interest as single crystal solid state lasers. Nevertheless only the YAG : Nd has achieved commercial importance. The YAG : Nd shows many advantages as to performance but some disadvantages, too, such as low solubility of Nd^{3+} in the YAG lattice, segregation of Nd^{3+} during crystal growth, limited tuning capability, etc. . . .

That means that it is more or less utopian to find a miracle material exhibiting all qualities: easy crystal growth, large conversion efficiency, good thermal conductivity, broad tuning range, . . . but, from a starting material, it is possible to make improvements leading to a high performance material for a particular property.

In this paper we shall show how these improvements can be realized. The starting laser material is the LMA : Nd (or LNA) discovered in 1980 in our laboratory (*2–4*).

The LNA Laser

The matrix LMA crystallizes with a hexagonal magnetoplumbite-like structure (MP). The structure of MP ($A^{2+}B^{3+}_{12}O_{19}$) belongs to the space group $P6_3/mmc$. The hexagonal unit cell is shown in Fig. 1(a). It consists of spinel blocks separated by mirror planes in which lie the large A^{2+} cations.

In the MP compounds ($A^{2+}B^{3+}_{12}O_{19}$) it is possible to substitute A^{2+} ions with trivalent ions of about the same size, especially with

[1] To whom correspondence should be addressed.

0022-4596/92 $3.00

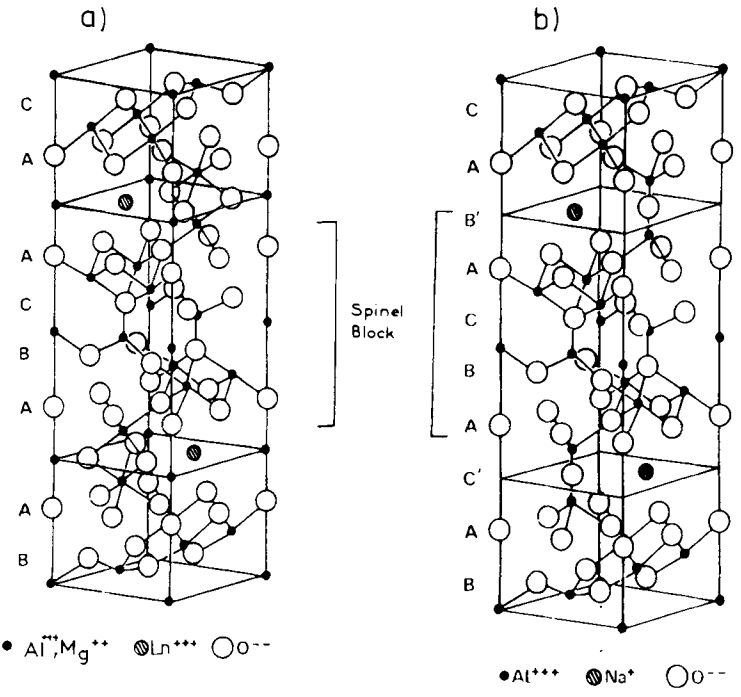

FIG. 1. The regular unit cell of: (a) $LaMgAl_{11}O_{19}$ with magnetoplumbite structure, (b) $NaAl_{11}O_{17}$ with β-alumina structure.

a lanthanide ion Ln^{3+} (*5*). The charge balance is realized by a substitution of a B^{3+} ion with a M^{2+} ion. For aluminates ($B^{3+} = Al^{3+}$; $M^{2+} = Mg^{2+}$) the total substitution leads to $Ln^{3+}Mg^{2+}Al_{11}^{3+}O_{19}$. In LMA : Nd Ln^{3+} is a mixed ion: $Ln^{3+} = (1 - x)La^{3+}$ (inactive ion) + xNd^{3+} (optically active ion). Finally, LNA is $La_{1-x}^{3+}Nd_x^{3+}Mg^{2+}Al_{11}^{3+}O_{19}$.

The fluorescence spectrum of Nd^{3+} in LNA shows two broad principal peaks associated with the transition $^4F_{3/2} \rightarrow {}^4I_{11/2}$ and centered at 1054 and 1082 nm (*4, 6*).

The yield of the fluorescence of Nd^{3+} as a function of x goes through a maximum for $0.1 < x < 0.2$ and the lifetime of the $^4F_{3/2}$ level is long (260 μsec for $x = 0.1$), indicating a weak self quenching of the emission (*2*).

The laser performance of LNA was studied for two crystals (*4*). The first one was 1 cm long with the crystal **c** axis parallel to the rod length. The second one was 2.4 cm long with its **a** axis parallel to the rod length. As a result of the strong anisotropy of the MP-like structure of LNA, the laser yield is 2 or 3 times higher when the rods are along the **c** axis. The optical pumping is less efficient at 514 nm (Ar^+ laser) than at 752 nm (Kr^+ laser) (Fig. 2). In this latter case, the slope efficiency is 26%, which corresponds to a quantum efficiency of 36%. These results are similar to those obtained with a rod of YAG : Nd 1%.

Finally, with respect to YAG : Nd, LNA has some advantages (*7*)

(i) higher neodymium content (2 to 6 times);

(ii) segregation coefficient of Nd^{3+} is close to 1, which allows homogeneous doping of the crystal in the whole composition range;

(iii) two emission lines which flank the

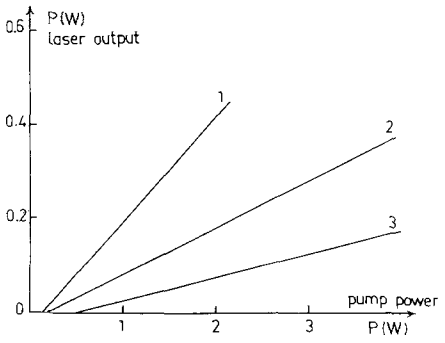

FIG. 2. Output power of the LNA laser as a function of the pump power, for 10% transmission of the output mirror: (1) and (2), crystal along **c** axis pumped respectively by a Kr^+ laser (λ = 752 nm) or an Ar^+ laser (λ = 514 nm); (3), crystal along **a** axis pumped by an Ar^+ laser.

YAG : Nd one (1.064 μm). The strongest one at 1.054 μm matches exactly with the maximum fluorescence of Nd^{3+} in phosphate glasses used as amplifiers in laser fusion devices. The second one at 1.082 μm can be used for nuclear polarization of helium atoms, which leads to numerous applications in nuclear physics and high sensitivity magnetometers;

(iv) however, the main characteristic of LNA is the broadness of its absorption and emission bands. It is possible to take advantage of the inhomogeneous broadened emission spectrum by inserting a Lyot filter in the laser cavity. The tuning of the laser emission can then be carried out over a range of 3.5 nm around the main line (1.054 μm) and over 8.0 nm around the 1.082 μm line. Fluorescence width in YAG under identical conditions is typically 0.6 nm.

Nevertheless LNA exhibits some disadvantages connected with its anisotropic structure and its thermal characteristics.

The next sections will show how the laser characteristics and performance of this family of materials can be modified and improved by making some convenient chemical modification of their formulas.

Improvement of the Laser Efficiency through Codoping

One of the most important limitations of the efficiency of Nd^{3+} solid state lasers is the lack of suitable strong absorption bands well matched to the spectral output of commercially available high power Kr or Xe lamps. The Nd^{3+} absorption spectrum consists of narrow lines of rather small oscillator strengths (*1*). A way to increase the pumping efficiency is to enhance the Nd^{3+} fluorescence by energy transfer from other doping ions. These sensitizer ions must have broad absorption bands well matched to the emission spectrum of the excitation lamp and a fluorescence emission overlapping the activator absorption lines. Cr^{3+} and Ce^{3+} have been used to sensitize Nd^{3+} fluorescence (*8, 9*).

(*a*) *Energy Transfer in LMA : Cr,Nd* (*10, 11, 13*)

Cr^{3+} ions can be partially substituted to Al^{3+} ions in the LMA matrix leading to a compound $La_{1-x}Nd_xMgAl_{11-y}Cr_yO_{19}$. These Cr^{3+} ions are mainly located in quasi-octahedral sites close to the mirror plane (*12*) where the Nd^{3+} ions lie.

The $Cr^{3+} \rightarrow Nd^{3+}$ energy transfer is clearly demonstrated by some experiments:

—study of fluorescence spectra of two crystals containing only chromium ions (Fig. 3(a)) and both Cr^{3+} and Nd^{3+} ions (Fig. 3(b)). These spectra were obtained by excitation at 640 nm. At this wavelength only Cr^{3+} absorbs so that the appearance of the Nd^{3+} fluorescence around 880 nm shows that the $Cr^{3+} \rightarrow Nd^{3+}$ energy transfer occurs

—study of decay profiles of LMA : Cr : Nd. For a given chromium content, the nonexponential character of the Cr^{3+} fluorescence decay increases and the

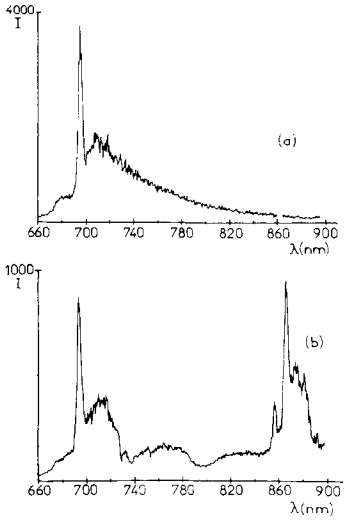

FIG. 3. Fluorescence spectra of LMA : 1.7×10^{20} Cr^{3+}/cm^3 (a) and LMA : 1.7×10^{20} Cr^{3+}/cm^3 – 2.6×10^{20} Nd^{3+}/cm^3 (b) (λ_{exc} = 640 nm). The spectra are corrected from monochromator and photomultiplier responses.

mean lifetime decreases when the neodymium concentration increases.

For the optimized concentrations in Cr^{3+} and Nd^{3+}, corresponding to $x = 0.14$ and $y = 0.05$, the transfer efficiency can reach 80 to 90%.

(*b*) *Energy Transfer in LMA : Ce,Nd (14, 15)*

Ce^{3+} ions can be incorporated into LMA. They substitute for La^{3+} ions in mirror planes. The absorption spectrum of Ce^{3+} in LMA covers well the UV emission range of the xenon arc-lamps. Furthermore, there is a good overlap between the Ce^{3+} emission band and the Nd absorption band. The transfer between Ce^{3+} and Nd^{3+} is clearly demonstrated by looking at the Ce^{3+} emission spectrum of LMA : Ce,Nd. The appearance of minima at wavelengths corresponding to Nd^{3+} absorption bands indicates that photons emitted by Ce^{3+} are reabsorbed by Nd^{3+}. The total intensity of the Ce^{3+} emission also decreases in the presence of Nd^{3+}. An estimation of the non-radiative $Ce^{3+} \rightarrow Nd^{3+}$ energy transfer efficiency can be deduced from the shortening of the Ce^{3+} lifetime for different Nd^{3+} concentrations in the matrix. In fact, the lifetime of Ce^{3+} is rather short (≅25 nsec). The non-radiative transfer leads to a maximum efficiency of about 47% for the studied composition range. It is significant but not very high compared to these for Cr → Nd transfer in LMA. This is related to the long distance Ce–Nd (both in mirror plane) compared to the shorter distance Cr (in spinel block)–Nd (in mirror plane).

(*c*) *Energy Transfer in LMA : Ce,Cr,Nd (15)*

This double sensitization system could combine the excitation of Ce^{3+} in the UV range and that of Cr^{3+} in the visible range. In a tridoped crystal, besides the $Ce^{3+} \rightarrow Nd^{3+}$ and $Cr^{3+} \rightarrow Nd^{3+}$ energy transfer one observes a strong interaction $Ce^{3+} \rightarrow Cr^{3+}$: the Ce^{3+} emission strongly decreases, mainly at long wavelengths, when the Cr^{3+} concentration increases (Fig. 4). In the same time, the lifetime of Ce^{3+} decreases when the Cr^{3+} concentration increases. The Ce → Nd,Cr non-radiative transfer is much more efficient than the transfer Ce → Nd.

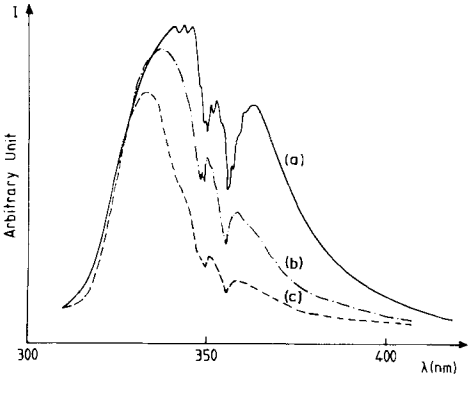

FIG. 4. Emission spectra under xenon lamp excitation of Ce^{3+} in $La_{0.9}Ce_{0.02}Nd_{0.08}MgAl_{11-x}Cr_xO_{19}$: (a) x = 0; (b) x = 0.055; (c) x = 0.11.

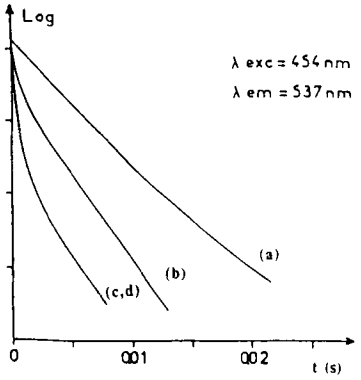

FIG. 5. Fluorescence decay profile of Mn^{2+} in LMA : Nd : Mn ($La_{1-y}Nd_yMg_{0.9}Mn_{0.1}Al_{11}O_{19}$) as a function of the neodymium content: (a) $y = 0$; (b) $y = 0.1$; (c) $y = 0.15$; (d) $y = 0.20$.

(d) Energy Transfer in LMA : S,Nd (S = Sensitizer Ion 3d or 4f)

Besides Cr^{3+} and Ce^{3+}, many other ions S are potential sensitizers of the Nd^{3+} fluorescence in LMA matrix. Some of them are located in spinel blocks, either in octahedral sites (Ti^{3+}) or in tetrahedral sites (Mn^{2+}); the others take place in the mirror plane (Eu^{2+}, Eu^{3+}, Tb^{3+}, Dy^{3+}), substituted to La^{3+}. The fluorescence emissions of these ions in LMA occur at different wavelengths (red and IR for Ti^{3+}, green for Mn^{2+}, blue for Eu^{2+}).

In almost all cases, one can observe a radiative and non-radiative transfer $S \rightarrow Nd^{3+}$. The transfer is demonstrated:

—by the appearance of minima of fluorescence at wavelengths corresponding to the absorption transitions of Nd^{3+};

—by a decreasing of the whole emission intensity of the sensitizer whose decay profile becomes less and less exponential when the activator concentration increases (Fig. 5).

The transfer yield is particularly high when $S = Ti^{3+}$, Mn^{2+}, Eu^{3+} ($\geq 80\%$). The transfer time is different for different sensitizers. For a laser application, some sensitizers would be more efficient in CW lasers (Mn^{2+}); others could be used both in pulsed and CW lasers (Eu^{3+}).

Improvement of Laser Efficiency through Crystal Growth. ASN New Laser Material

As mentioned above (Fig. 2), the laser efficiency of the anisotropic LNA is highest when the rod axis is parallel to the **c** axis of the crystal. Unfortunately, the growth of LNA single crystals by the Czochralski technique along the **c** axis is very difficult because the crystal presents a perfect cleavage plane (00.1). The spontaneous growth axis is the **a** axis. It is possible to use a **c**-oriented seed, but the main problem is to preserve this orientation during the whole pulling-process. Nevertheless, by a drastic control of all parameters of the crystal growth, J. J. Aubert and co-workers succeeded in growing large **c**-oriented crystals (*16*).

More recently, we discovered a new laser material belonging to the MP type and showing an interesting growing characteristic (*17, 18*). In the MP-like aluminate $A^{2+}Al_{12}^{3+}O_{19}$ the total substitution of A^{2+} with a lanthanide ion Ln^{3+} (and in the same time substitution of Al^{3+} with Mg^{2+}) leads to LMA $Ln^{3+}Mg^{2+}Al_{11}^{3+}O_{19}$. When the substitution is partial, the same mechanism leads to a compound $A_{1-x}^{2+}Ln_x^{3+}Mg_x^{2+}Al_{12-x}^{3+}O_{19}$ ($A^{2+} = Ca^{2+}$ or Sr^{2+}). When $A^{2+} = Sr^{2+}$ and $Ln^{3+} = Nd^{3+}$, we obtain a strontium neodymium aluminate $Sr_{1-x}^{2+}Nd_x^{3+}Mg_x^{2+}Al_{12-x}^{3+}O_{19}$ referred to as ASN.

The fluorescence characteristics of ASN are similar to those of LNA. For the same transition ($^4F_{3/2} \rightarrow {}^4I_{11/2}$), the fluorescence intensity goes through a maximum for $x \cong 0.4$, and the lifetime of the $^4F_{3/2}$ level is long (170 μsec for $x = 0.2$).

Because of the vicinity of the structures of the two compounds LNA and ASN, one can think that the laser efficiency would be higher when the **c** axis of the crystal is paral-

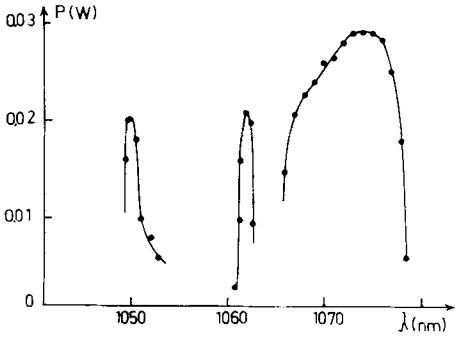

FIG. 6. Tuning range of the laser emission of $Sr_{0.8}Nd_{0.2}Mg_{0.2}Al_{11.8}O_{19}$ under argon ion laser excitation (514 nm).

lel to the axis of the laser rod. A main difference between the 2 compounds appears: the crystal of ASN grows spontaneously along the **c** axis, even when the crystal growth is carried out without seed. Under 514.5 μm excitation, free running laser emission was observed at 1049.8 nm with an efficiency of 21% for a 10% transmitting output mirror. Two other lines were observed at 1061.8 and 1074 nm.

Besides this very interesting crystal growth characteristic (spontaneous growth along the most favorable direction for laser emission), ASN shows another advantage with respect to LNA. The tunability range (Fig. 6) around the two first emission lines is narrow (1.5 nm) but around 1074 nm it reaches 12 nm. This is the largest tunability range reported so far, to our knowledge, for a Nd^{3+} activated single crystalline laser material.

Improvement of Thermal Behavior. STON Effect

The most important disadvantage of LNA against YAG is its rather low thermal conductivity, which is about half that of YAG. As a result of that, temperature gradients between the center and the outside of the laser rod are important, and they induced thermal focusing effects by variation of the refractive index (*19*). The pumped rod is equivalent to a thick lens with pump dependence of the focal length. We compared two LMA crystals, one Nd^{3+} doped and the other Cr^{3+}, Nd^{3+} double-doped, at a given pump power (Fig. 7). The focal length is higher in the codoped crystal and therefore the thermal focusing effect is weaker. The presence of Cr^{3+} ions considerably increases the average absorption coefficient for the pumping light (the oscillator strength of Cr^{3+} is about 100 times higher than that of Nd^{3+}). An important part of the lamp emission power is absorbed in a thin layer from the rod surface and partially converted into heat. An enhancement of the heating effect close to the surface can be assumed. This leads to a smoothing of the temperature and hence to a weaker refractive effect of the laser beam. This effect is known in other materials and described as STON effect (smoothing of thermooptical inhomogeneties) (*20*).

Therefore, the codoping of crystals is interesting not only to improve the efficiency but also to avoid focusing effects in laser

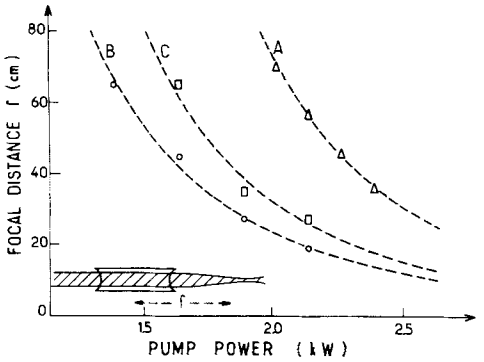

FIG. 7. Thermal focusing effects under lamp pumping excitation for three LMA rods 105 mm in length, 5 mm in diameter, cut along the **a** axis: (A) LMA : Cr,Nd crystal (4% Nd, 1% Cr), end faces with a 60 cm radius of curvature; (B) LMA : Nd crystal (15% Nd), 60 cm radius; (C) LMA : Nd crystal (15% Nd), 45 cm radius.

materials exhibiting poor thermal conductivity.

Tunable Laser Materials with LMA Matrix

As mentioned before, LNA and ASN lasers exhibit an unusually broad range of tunability for lanthanide activated lasers. But the most promising tunable lasers are those activated with *d* transition metal ions (*7, 21*). In this field Ti^{3+} is particularly interesting because of its very simple electronic structure, the lack of excited state absorption, and the broad fluorescence band leading to the broadest tuning range known for a transition ion-activated laser (≅400 nm). Presently the only commercial titanium-activated laser is the titanium doped sapphire ($Al_2O_3 : Ti^{3+}$) (*21, 22*). Its disadvantages are the segregation and the low solubility of titanium ($Ti/Al \leq 3\ 10^{-3}$) (*23, 24*).

LMA : Ti could be a new potential tunable laser (*25, 26*). The solubility of Ti is significantly higher in LMA than in Al_2O_3 matrix ($Ti^{3+}/Al^{3+} \leq 1/10$). Ti ions exist in both 3+ and 4+ oxidation states and also probably as Ti^{2+} due to the dismutation $2\ Ti^{3+} \rightarrow Ti^{2+} + Ti^{4+}$. These ions are shared among the three kinds of octahedral sites of the LMA unit cell, the distribution depending upon the titanium content (*28*).

The emission spectrum of LMA : Ti exhibits 2 bands around 730 and 960 nm in addition to the *d–d* band of Ti^{3+} around 550 nm (*26, 27*). These bands are annoying because they occur in the same wavelength range as the Ti^{3+} fluorescence in LMA. A careful study carried out on a lot of crystals prepared under different oxidizing and reducing treatments (*28, 29*) shows that:

(i) these bands are associated with the presence of titanium in a reduced state;

(ii) the transitions responsible for the bands cannot arise from single ions. They may originate from an optical intervalence charge transfer transition (IVCT) (*29*). In fact, the bands occur in a wavelength range where IVCT have already been observed in other materials (*30, 31*);

(iii) the 730-nm band may correspond to a Ti^{3+}–Ti^{4+} transfer and could be suppressed by elimination of Ti^{4+}; the 960-nm band is tentatively attributed to a Ti^{2+}–Ti^{3+} transfer and could perhaps be suppressed by a careful control of oxidation–reduction treatments preventing the formation of Ti^{2+}.

Fluorescence spectra of Ti^{3+} in LMA : Ti show a broad band going from 650 to beyond 850 nm (the cutoff of our spectrometer).

In conclusion LMA : Ti will be a very interesting tunable laser material when the parasitic absorption bands have been eliminated.

LMA-Based Laser Materials for Visible or NIR (1.5–3 μm) Emission

In the field of solid state lasers, there has been renewed attention in recent years for activator ions other than Nd^{3+}. Among these ions, the most widely studied were Pr^{3+} for its fluorescent lines in the visible range, Ho^{3+} which gives rise to laser action at about 2.1 μm, and Er^{3+} whose laser emissions occur at about 1.5 and 2.8 μm. There are specific applications for lasers at these wavelengths (*1, 7, 32*).

The absorption and fluorescence of Pr^{3+}, Ho^{3+}, and Er^{3+} in LMA single crystals have been studied in order to determine whether these activated LMA had specific properties for laser applications.

Single crystals of $La_{1-x}Ln_xMgAl_{11}O_{19}$ (LMA : *Ln*) were grown by the Verneuil method. For Pr^{3+}, x can be varied continuously from 0 to 1. On the contrary, Ho and Er form garnets and not magnetoplumbites. Therefore, the x values corresponding to the solubility limit are only 0.14 and 0.10, respectively (*33*).

The main Pr^{3+} fluorescence band occurs at about 490 nm and corresponds to the

$^3P_0 \rightarrow {}^3H_4$ transition. Other weaker lines corresponding to transitions from $^3P_0$ to $^3H_{5,6}$, $^3F_{2,3,4}$ and from $^1D_2$ to $^3H_{5,6}$ are also observed.

Broad band lamp pumping of Pr^{3+} is difficult because there are only a few energy levels above the fluorescent ones. Therefore attempts have been made to sensitize the Pr^{3+} emission in LMA by codoping either with Dy^{3+} which has $^4F_{9/2} \rightarrow {}^6H_{15/2}$ fluorescence in resonance with $^3H_4 \rightarrow {}^3P_{0-2}$ Pr^{3+} absorption, or with Sm^{3+} which gives a strong orange emission in this matrix ($^4G_{5/2} \rightarrow {}^6H_{7/2}$ transition) matching the $^3P_0 \rightarrow {}^1D_2$ Pr^{3+} absorption.

However, there is no strong decrease of the Dy fluorescence intensity in doubly doped LMA. Furthermore the excitation spectrum of LMA : Pr : Dy contains only Pr^{3+} absorption lines (*34*). Similar results are obtained for Sm^{3+} codoping.

It follows that Pr^{3+} sensitization, if any, is poorly efficient. Furthermore, the Pr^{3+} strongest emission line is towards the ground state and therefore an LMA : Pr laser should work on a three-level scheme. It can be concluded that LMA : Pr will probably not be a good laser material.

Preliminary investigation of the optical properties of LMA : Ho and LMA : Er single crystals have also been performed (*33, 35*). Both crystals exhibit strong absorption lines which are suitable for optical pumping. The shape of the absorption and emission bands depends upon the dopant concentration. An example of such behavior is given in Fig. 8 for LMA : Ho fluorescence around 2 μm. This can be understood owing to the multisite character of the lanthanide localization in the LMA matrix (*5*). When the holmium rate increases, a second Ho site begins to populate, leading to new emission lines. The broadness of the 2 μm band should allow the tuning of the laser emission in the 1.9 to 2.1 μm range.

Single crystals of LMA : Ho of good optical quality have been grown recently by the Czochralski method. Laser tests will be performed in the near future.

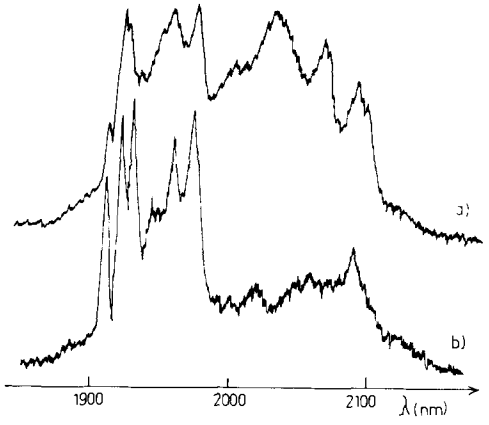

FIG. 8. 100 K emission spectra corresponding to $^5I_7 \rightarrow {}^5I_8$ transition of Ho^{3+} in LMA : Ho for two doping levels: (a) $x = 0.1$; (b) $x = 0.015$.

A New Way of Activating Solids: Lanthanide Ion Exchange in Sodium β-Aluminogallates

Sodium β-aluminogallates single crystals with good optical quality, typically 5 × 5 × 1.5 mm^3 in size, can be grown by flux evaporation in NaF (*36*). These compounds, with formulas $Na_{1+x}(Al_{1-y}Ga_y)_{11}O_{17+x/2}$ ($0.25 \leq y \leq 0.7$ and $x \cong 0.7$), have the β-alumina structure shown Fig. 1(b). Like MP structure (Fig. 1(a)), the β-alumina one is made of spinel blocks separated by mirror planes containing sodium ions. The latter are called conduction planes because they are loosely packed and allow fast migration of the sodium ions, leading to the well known ionic conduction properties of this material. In β-alumina, sodium ions can be replaced by other mono- or divalent cations by ion exchange in molten salts (*37*). However, lanthanide ion exchange does not occur. We have found that with partial substitution of aluminium by gallium in the β-alumina lattice, leading to aluminogallates

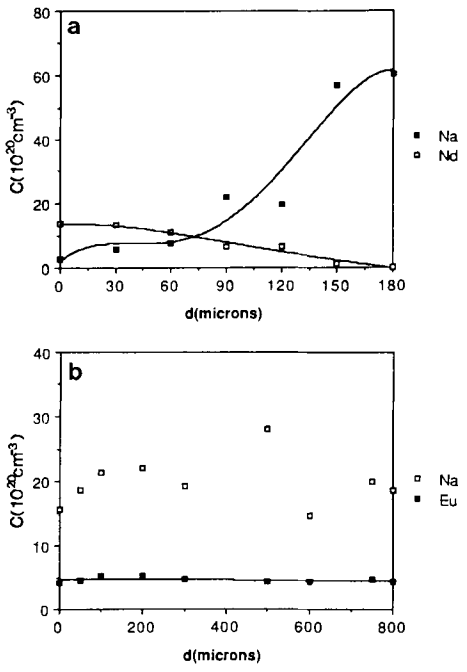

FIG. 9. Examples of rare earth and sodium concentration profiles, from the edge toward the center of the crystals, in partially exchanged aluminogallates. The experimental conditions were the following; (a) 1 hr in $NdCl_3$ at 810°C; (b) 16 hr in 40 $EuCl_3$/60 NaCl at 650°C.

which are studied here, the sodium–lanthanide ion exchange becomes possible. This is performed by immersing the sodium aluminogallate crystals in molten $LnCl_3$ or $LnCl_3$–NaCl mixtures (650–850°C) for 30 min to 16 hrs (*36*). Depending upon the particular lanthanide ion (*Ln*) and exchange procedure, the lanthanide ion distribution can be homogeneous or not, as revealed by examples of the concentration profiles given Fig. 9.

The different behavior, with respect to lanthanide ion exchange, of the β-alumina and aluminogallates can be understood from the structure refinement of the β-aluminogallates (*38*). The large gallium ions (compared to Al^{3+}) are located mainly in the tetrahedral sites. Some of them, close to the conduction plane, enlarge the spacing between the spinel blocks which are on each side of the conduction plane, thus making sodium migration easier. Furthermore, the sodium ions are much more disordered, probably because the potential wells along the conduction path are less deep. This could also favor ion exchange.

Among the lanthanide exchanged β-aluminogallates, those activated with neodymium are of particular interest. Their optical absorption spectra are rather unusual (*39*), being dominated by the very strong hypersensitive band near 580 nm whose oscillator strength is 37×10^{-6} (Fig. 10).

The $^4F_{3/2}$ excited state lifetime, 450 μsec for a neodymium concentration of $\cong 10^{21}$ ions cm^{-3}, is also very high, indicating that the self quenching of the fluorescence is very weak in this material. Neodymium β-aluminogallate could therefore be an interesting optronic material for integrated optics, like its parent compound neodymium β″-aluminate (*40*).

Compared with the usual way of activating the optical properties of single crystals (doping in the molten state before pulling the crystals), ionic exchange offers several advantages:

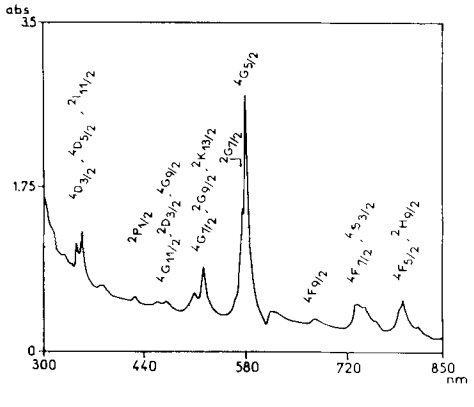

FIG. 10. 300 K absorption spectrum of Nd^{3+} in partially exchanged sodium β-aluminogallate showing the strong $^4I_{9/2} \rightarrow {}^4G_{5/2}, {}^2G_{7/2}$ hypersensitive transition.

(i) synthesis of numerous samples with various activators and doping levels from the same batch of starting crystals;

(ii) preparation of metastable compounds (but which discompose only above 1000°C) which may present unusual properties. These compounds cannot be obtained by the usual procedures which follow the thermodynamical equilibrium laws;

(iii) possibility to obtain doubly doped samples, either by single ion exchange of crystals already doped in the spinel blocks (at the stage of crystal growth) or by ion exchange with appropriate mixture of molten salts.

Preliminary investigation of codoped crystals indicates that efficient energy transfer occurs between Cr^{3+} and Nd^{3+} in crystals obtained by the first way (*41*). However, the second process of codoping appears even more promising, according to recent results obtained with β''-alumina coexchanged with Yb^{3+} and either Er^{3+}, Ho^{3+}, or Tm^{3+}. These crystals can be diode pumped through Yb^{3+} absorption, and show, for instance, infrared to visible luminescence upconversion (*42*).

Acknowledgments

The authors are grateful to Drs. G. Aka, A. Kahn-Harari, A. M. Lejus, J. Théry, and B. Viana who have participated in the work summarized in this paper and to P. Aschehoug, J. M. Benitez, D. Serreau, and D. Simons for their technical assistance in performing the experiments or preparing this manuscript.

References

1. A. A. Kaminskii, "Laser Crystals," Springer, Berlin/New York (1981).
2. A. Kahn, A. M. Lejus, M. Madsac, J. Théry, D. Vivien, and J. C. Bernier, *J. Appl. Phys.* **52,** 6864 (1981).
3. D. Vivien, A. M. Lejus, J. Théry, R. Collongues, J. J. Aubert, R. Moncorgé, and F. Auzel, *C.R. Acad. Sci.* **298,** 195 (1984).
4. L. D. Schaerer, M. Leduc, D. Vivien, A. M. Lejus, and J. Théry, *J. Quantum Electron.* **5,** 713 (1986).
5. R. Collongues, D. Gourier, A. Kahn-Harari, A. M. Lejus, J. Théry, and D. Vivien, *Annu. Rev. Mater. Sci.* **20,** 51 (1990).
6. V. M. Garmash, A. A. Kaminskii, H. I. Polyakov, S. E. Sarkisov, and A. A. Filimonov, *Phys. Status Solidi* **75,** 111 (1983).
7. D. Vivien, *Rev. Phys. Appl.* **21,** 709 (1986).
8. S. A. Payne and L. L. Chase, *J. Opt. Soc. Am.* **B3,** 1181 (1986).
9. R. M. Brewer and M. Nicol, *J. Lumin.* **21,** 367 (1980).
10. B. Viana, C. Garapon, A. M. Lejus, and D. Vivien, *J. Lumin.* **47,** 73 (1990).
11. C. G. Aminoff, C. Larat, M. Leduc, B. Viana, and D. Vivien, *J. Lumin.* **50,** 21 (1991).
12. B. Viana, A. M. Lejus, D. Vivien, V. Ponçon, and G. Boulon, *J. Solid State Chem.* **71,** 77 (1987).
13. R. I. Gentoft, A. M. Zabaznov, N. M. Paltarak, and A. P. Shkadarevich, *J. Appl. Spectrosc.* **48,** 233 (1988).
14. B. Viana, G. Aka, D. Vivien, A. M. Lejus, J. Théry, A. Derory, J. C. Bernier, C. Garapon, and G. Boulon, *J. Appl. Phys.* **64,** 1398 (1988).
15. B. Viana, C. Garapon, A. M. Lejus, and D. Vivien, *J. Mater. Sci.* in press.
16. C. Wyon, J. J. Aubert, and Y. Grange, *J. Cryst. Growth* **99,** 845 (1990).
17. S. Alablanche, J. M. Benitez, R. Collongues, J. Théry, and D. Vivien, French patent 9003180 (1990).
18. R. Collongues, S. Alablanche, A. M. Lejus, J. Théry, D. Vivien, J. J. Aubert, and C. Wyon, "Eur. Conf. on Crystal Growth, Budapest (1991)."
19. W. Koechner, *Appl. Opt.* **9,** 1429 (1970).
20. I. A. Scherbakov, *IEEE J. Quantum Electron.* **QE 24,** 979 (1988).
21. A. B. Budgor, L. Esterowitz, and L. G. Deshazer, Eds., "Proceedings, Tunable Laser Conference II, Zigzag (USA), Springer, Berlin (1986).
22. R. Moncorgé, G. Boulon, D. Vivien, A. M. Lejus, R. Collongues, V. Djevahirdjian, K. Djevahirdjian, and R. Cagnard, *J. Quantum Electron.* **24,** 6 (1988).
23. S. K. Mohapatra and F. A. Kroger, *J. Am. Ceram. Soc.* **60,** 381 (1977).
24. N. E. Kask, L. S. Kornienko, T. S. Mandel Sham, and A. M. Prokhorov, *Sov. Phys. Solid State* **5,** 1677 (1964).
25. D. Gourier, L. Colle, A. M. Lejus, D. Vivien, and R. Moncorgé, *J. Appl. Phys.* **63,** 1144 (1988).
26. C. Wyon, J. J. Aubert, D. Vivien, A. M. Lejus, and R. Moncorgé, *J.Lumin.* **40,** 871 (1988).
27. X. Jiang, Y. Jiang, J. Liang, H. Xia, and Y. Chen, *J. Cryst. Growth* **97,** 761 (1989).

28. B. MARTINAT, A. M. LEJUS, AND D. VIVIEN, *Mater. Res. Bull.* **25,** 52 (1990).
29. B. MARTINAT, D. GOURIER, A. M. LEJUS, AND D. VIVIEN, *J. Solid State Chem.* **89,** 147 (1990).
30. M. G. TOWNSEND, *Solid State Commun.* **6,** 81 (1968).
31. S. REISFELD, M. EYAL, AND C. K. JORGENSEN, *Chimica,* **41,** 117 (1987).
32. "Proceedings of the French-Israeli Workshop on Solid State Lasers" (G. Boulon, C. K. Jorgensen, and R. Reisfeld, Eds.), SPIE Vol 1182 (1989).
33. B. VIANA, P. DEROUINEAU, L. GERVAT, D. VIVIEN, AND A. M. LEJUS, *J. Appl. Phys.* **52,** 225 (1981).
34. B. VIANA, P. DEROUINEAU, J. BARRIE, A. M. LEJUS, B. DUNN, O. STAFSUDD, AND D. VIVIEN, *J. Phys.* **48,** C7-509 (1987).
35. B. VIANA, D. VIVIEN, A. M. LEJUS, C. WYON, AND J. J. AUBERT, *Eur. J. Solid State Inorg. Chem.* **27,** 869 (1990).
36. G. AKA, J. THÉRY, AND D. VIVIEN, *Solid State Ionics* **39,** 225 (1990).
37. Y. F. YAO AND J. T. KUMMER, *J. Inorg. Nucl. Chem.* **29,** 2453 (1967).
38. A. KAHN-HARARI, G. AKA, AND J. THÉRY, *J. Solid State Chem.* **91,** 71 (1991).
39. G. AKA, J. THÉRY, AND D. VIVIEN, *J. Electrochem. Soc.* Nov. 1991 in press.
40. M. JANSEN, A. ALFREY, O. M. STAFSUDD, B. DUNN, D. L. YANG, AND G. C. FARRINGTON, *Opt Lett.* **9,** 119 (1984).
41. J. THÉRY, G. AKA, V. LUCAS, C. SAYAG, B. VIANA, AND D. VIVIEN, *Ann. Phys. Paris,* **16** Colloque n°2, 221 (1991).
42. B. VIANA, L. A. MOMODA, AND B. DUNN, "2nd Laser M2P Conference, Grenoble (France) July (1991)."